

Energy & Environmental Science

Accepted Manuscript



This is an *Accepted Manuscript*, which has been through the Royal Society of Chemistry peer review process and has been accepted for publication.

Accepted Manuscripts are published online shortly after acceptance, before technical editing, formatting and proof reading. Using this free service, authors can make their results available to the community, in citable form, before we publish the edited article. We will replace this *Accepted Manuscript* with the edited and formatted *Advance Article* as soon as it is available.

You can find more information about *Accepted Manuscripts* in the [Information for Authors](#).

Please note that technical editing may introduce minor changes to the text and/or graphics, which may alter content. The journal's standard [Terms & Conditions](#) and the [Ethical guidelines](#) still apply. In no event shall the Royal Society of Chemistry be held responsible for any errors or omissions in this *Accepted Manuscript* or any consequences arising from the use of any information it contains.

Single Layer Graphene Encapsulating Non-Precious Metals as High-performance Electrocatalysts for Water Oxidation

Xiaoju Cui[†], Pengju Ren[†], Dehui Deng^{*}, Jiao Deng, Xinhe Bao^{*}

State Key Laboratory of Catalysis, *i*ChEM, Dalian Institute of Chemical Physics, Chinese Academy of Sciences, Zhongshan Road 457, Dalian, 116023, China.

[†]These authors have contributed equally.

*E-mail: dhdeng@dicp.ac.cn; xhbao@dicp.ac.cn; Fax: +86-411-84379128; Tel: +86-592-2186917

Abstract

Oxygen evolution reaction (OER) is recognized as a key half-reaction in water electrolysis for clean hydrogen energy, which is kinetically not favored and usually requires precious metal catalysts such as IrO₂ and RuO₂ to reduce the overpotential. The major challenge in using non-precious metals to replace these precious metal catalysts for OER is their low efficiency and poor stability, which urgently demands new concepts and strategies to solve this issue. Herein, we report a universal strategy to directly synthesize single layer graphene encapsulating uniform earth-abundant 3d transition-metal nanoparticles such as Fe, Co, Ni and their alloys in a confined channel of mesoporous silica. The single atomic thickness of graphene shell immensely promotes the electron transferring from the encapsulated metals to the graphene surface, which efficiently optimizes the electronic structure of the graphene surface and therefore triggers the OER activity of the inert graphene surface. We investigated a series of non-precious 3d metals encapsulated within single layer graphene, and found that the encapsulated FeNi alloy showed the best OER activity in alkaline solutions with only 280 mV overpotential at 10 mA cm⁻², and also possessed a high durability after 10 000 cycles. Both the activity and durability of the non-precious catalyst even exceed that of commercial IrO₂ catalyst, showing great potential to replace precious metal catalysts in OER.

Keywords: electrocatalysis · graphene · non-precious metals · water oxidation reaction · electron transfer

Context

The increasing demand for clean energy and diminishing fossil energy resources are stimulating intense research interest in developing earth-abundant energy alternatives and designing efficient energy-storage devices¹⁻⁵. Among many innovative approaches, the production of hydrogen through electricity-driven water splitting has attracted great attention in recent years. The oxygen evolution reaction (OER), as a key half-reaction involved in water splitting, is kinetically not favored and requires a catalyst to expedite the reaction⁶⁻¹⁰. Precious metal catalysts such as IrO₂ and RuO₂ are the state-of-the-art OER electrocatalysts¹¹⁻¹³, while their applications are hindered due to their high cost and scarcity. Consequently, tremendous research efforts have been devoted to developing non-precious metal catalysts. Particularly, earth-abundant 3d transition metals (TMs) like Fe, Co and Ni have been considered as promising catalytic materials for replacement of precious catalysts due to their high theoretical activity and low cost¹⁴⁻¹⁹. However, bare 3d TMs catalysts are not stable enough when they suffer the long-time operation or accelerated degradation measurements under strong alkaline electrolytes and high overpotential.

Recently, we proposed a strategy to construct a series of 3d TMs encapsulated into carbon nanotubes or graphitic carbon shells to prevent the corrosion of 3d TMs from the harsh environment and simultaneously promote the catalytic reaction on carbon surface due to the electron transfer from encapsulated 3d TMs²⁰⁻²⁴. This strategy was proved efficiently by different research groups in a series of reactions, such as oxygen reduction reaction (ORR)^{20, 24-26} in fuel cells, hydrogen evolution reaction (HER)^{21, 22, 27, 28} in water electrolysis and triiodide reduction reaction in the dye-sensitized solar cells (DSSCs)²⁹ as well as catalytic oxidation and reduction reactions in heterogeneous catalysis^{30, 31}. Previous studies indicated that too thick carbon shell would obstruct the electron transfer from the metals to the carbon and subsequently decrease the catalytic activity on carbon surface^{21, 24}. Moreover, the electron transfer significantly rely on the work function of different metals and their interaction strength with graphene^{20, 32-36}. Therefore, it is significative to develop a universal method to reduce the layer number of graphitic carbon and meanwhile achieve the encapsulation of all kinds of metals.

Herein, we introduced a facile and universal method for the preparation of single layer graphene encapsulating uniform 3d TMs, including Fe, Co, Ni and their alloys nanoparticles (NPs) via a chemical vapor deposition (CVD) process in the channel of ordered mesoporous silica (SBA-15). As shown in Fig 1, firstly, metal-containing precursors were filled into the channel of SBA-15 (with a pore size distribution of 7-9 nm) by an impregnation method in methanol solution, and then the samples were heated to 700 °C under H₂, followed by a CVD of carbon source (acetonitrile) on the metal NPs formed at high temperature. Due to the confinement of SBA-15 channel, the metal precursors can firstly form uniform particles under high temperature, and the single layer graphene will be formed between the metal nanoparticles surface and pore walls of SBA-15. Hence, the single layer graphene will grow on the surface of the metal NPs in the channel of SBA-15, and a small quantity of multi-walled carbon nanotubes (CNTs) will grow on the residual metal NPs outside SBA-15. The final single layer graphene encapsulating metal NPs on the interlaced CNTs can be obtained after etching SBA-15 and bare metals by HF solution. Through the method, a series of single layer graphene encapsulating 3d TMs (M@NCs) can be easily prepared, denoted as Fe@NC, Co@NC, Ni@NC, FeCo@NC, FeNi@NC and CoNi@NC, respectively, according to the metal types (see Experimental Section in Supporting Information for more details).

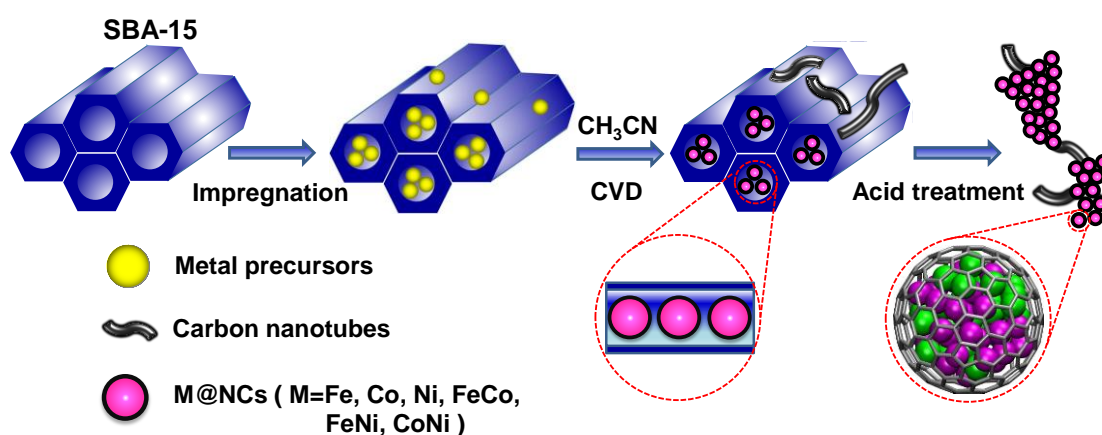


Fig 1. Schematic illustration of the synthesis process of M@NCs from the metal-containing precursors and SBA-15.

High-resolution transmission electron microscopy (HRTEM), X-ray diffraction

(XRD) and X-Ray photoelectron spectroscopy (XPS) were employed to characterize the structural and electronic properties of the obtained M@NCs. Take the FeNi@NC sample as an example, the HRTEM images of the unpickled sample (FeNi@NC/SBA-15) clearly show numerous small NPs inside the ordered mesoporous channel of SBA-15 (Figure 2a) after the CVD process, which should correspond to the graphene encapsulating FeNi NPs. After the removal of SBA-15, one can see uniform metal NPs with an average diameter of 6-10 nm distributed on the interlaced CNTs (Fig 2b-c, S1, S2a). Further HRTEM analysis (Fig 2c-d, S2b) indicates that the metal NPs were completely encapsulated by the graphene layer with a layer thickness of around 3.4 Å, which corresponding to the single layer graphene. According to the statistics analysis of more than 300 HRTEM pictures (Fig 2b), almost 98.5% graphene layer on FeNi NPs are single layer. In addition, these NPs exhibit a d spacing of 2.1 Å, in good agreement with the (111) plane of the FeNi alloy. The crystal structure of FeNi alloy NPs was further confirmed by XRD (Fig 2e), which shows the characteristic peaks at 51.8° and 76.4°, corresponding to the (200) and (220) planes of the FeNi alloy, respectively. Note that the 26.5° peak in the XRD patterns should originate from C (002) of multi-walled CNTs. The chemical states of these NPs by XPS (Fig 2f) also suggest that both Fe and Ni in FeNi@NC keep their metallic state, which was consistent with the XRD analysis and HRTEM results. The metallic characteristics of these NPs further prove that FeNi NPs are completely encapsulated within the single layer graphene shell, preventing the oxidation of the FeNi alloy when exposed to air. Likewise, the encapsulation of other metallic Fe, Co, Ni, FeCo and CoNi alloy within single graphene layer were also confirmed by the similar characterizations in the supporting materials (Fig S3-12). These results indicate that a series of uniform 3d NPs and their corresponding alloys have been successfully encapsulated in single layer graphene shell by using the facile method.

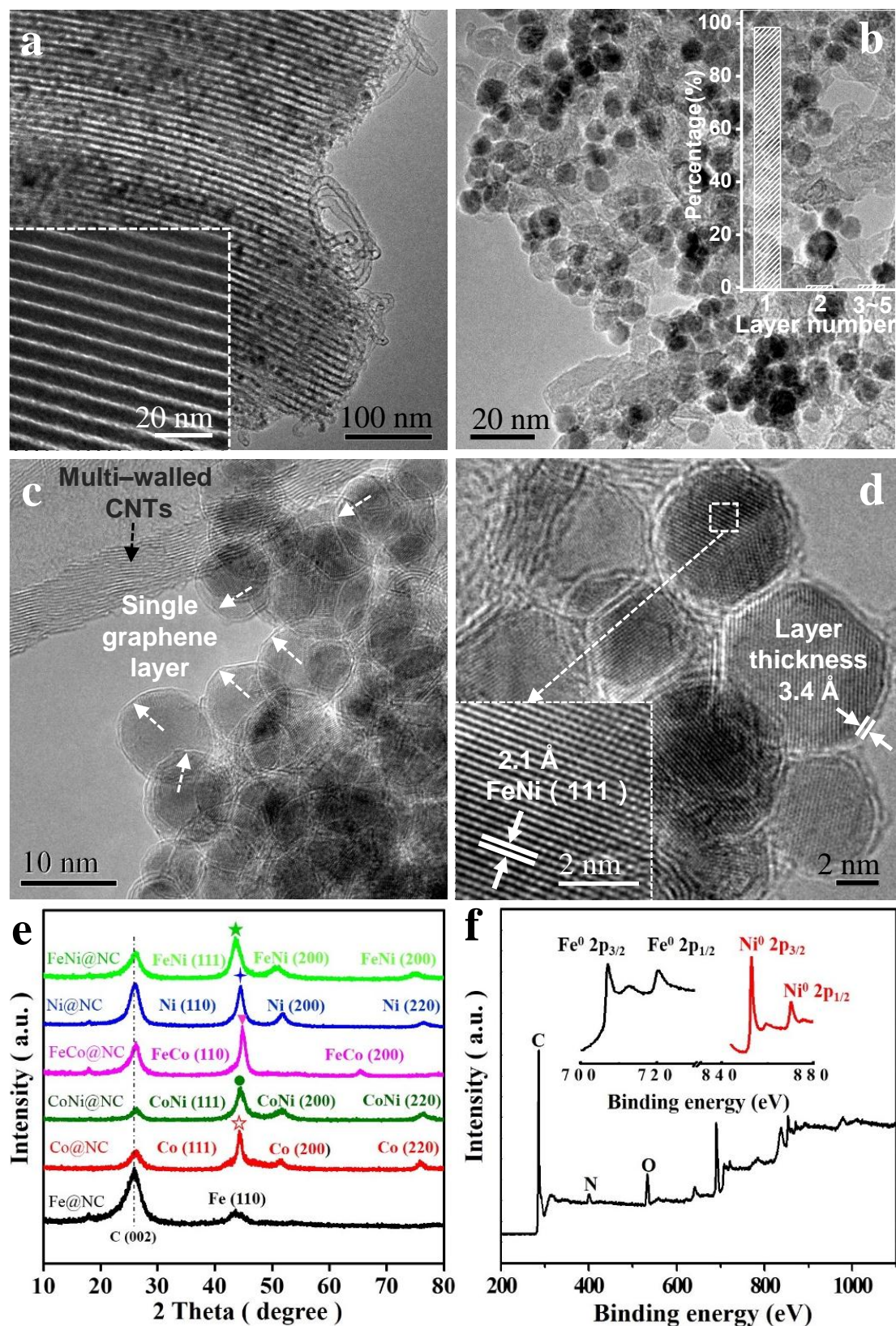


Figure 2. Morphology and structural characterizations of M@NCs. (a) TEM images of FeNi@NC/SBA-15, showing the metal NPs inside the channel of SBA-15 and a small

quantity of CNTs outside SBA-15. The insert is an image of pure SBA-15. (b-d) HRTEM images of FeNi@NC. The inset in (b) is a statistical analysis of layer number of the graphene shell on metal nanoparticles. The white arrows inset in (c) showing the single layer graphene, and the black arrow inset in (c) showing the multi-walled carbon nanotubes. The inset in (d) showing the (111) crystal plane of FeNi alloy and the graphene layer with a layer thickness of 3.4 Å. (e) XRD patterns of different M@NCs. (f) Fe 2p and Ni 2p XPS spectra of FeNi@NC sample.

A typical three-electrode electrochemical cell was adopted to evaluate the OER performance of these M@NCs catalysts in 1 M NaOH solution. As shown in Figure 3a, linear sweep voltammograms (LSV) were carried out to evaluate the OER performance of these M@NCs catalysts. As references, we also carried out the measurements of pure CNTs, few-layer graphene nanosheets and IrO₂. The polarization curves showed that all these M@NCs catalysts had much higher OER activity than pristine CNTs and graphene nanosheets (Fig S15a). The trend of the overpotential at the same current density 10 mA cm⁻² is FeNi@NC < CoNi@NC < FeCo@NC < Ni@NC < Fe@NC < Co@NC (Fig S15c), indicating that FeNi@NC possessed the best OER activity among these M@NCs catalysts. By analyzing the BET surface area of M@NCs catalysts (Table S1), we find that there is not a direct relation between activity and surface area. Besides, the N content in these samples is similar according to the element analysis (Table S3, S4). Hence, the difference of the activity for these samples should mainly originate from the different metal types. More interestingly, the onset potential of FeNi@NC sample is only 1.44 V vs. RHE, and the potential at 10 mA cm⁻² and 20 mA cm⁻² were 1.51 V vs. RHE and 1.54 V vs. RHE, respectively (Fig 3a), which is even better than that of commercial IrO₂. It is also one of the most active catalysts for OER in the recent reports (Table S9). To gain additional insights into the OER process on FeNi@NC, the Tafel plots of the potential vs. log (current density) were recorded (Fig 3b) with their linear portions at low potential fitted to the Tafel equation. The Tafel slope of FeNi@NC sample was 70 mV dec⁻¹, which is comparable to the value 63 mV dec⁻¹ of IrO₂, showing FeNi@NC sample possessed the similar ability to drive the OER

process compared to IrO₂ at low overpotential. Durability is another critical parameter to evaluate the performance of non-precious-metal electrocatalysts in OER. In this study, the accelerated degradation test was employed to evaluate the durability. The polarization curve for OER was recorded after every 1000 cyclic voltammetric (CV) sweeps between -0.46 and 0.54 V (vs. Hg/HgO) at 100 mV s⁻¹. One can see the polarization curve of FeNi@NC after 10 000 cycles retained an almost similar performance to the initial test (Fig 3c). A slight peak emerging around 1.5 V vs. RHE may be ascribed to the oxidation of Ni^{II} to Ni^{III}, which is probably caused by a small quantity of exposed FeNi nanoparticles, because some graphene layer may be destroyed during the long-term accelerated degradation test in the strong alkaline electrolyte. In contrast, the activity of IrO₂ decayed quickly with the same accelerated degradation test. Moreover, from the potential values recorded at different current densities of 40 mA cm⁻² and 100 mA cm⁻² before and after the test, FeNi@NC exhibited high durability with only a slight increase at the potential (Fig 3d), obviously superior to the durability of commercial IrO₂. Note that both the structure of the single layer graphene and the encapsulating FeNi nanoparticles were still well maintained after the OER durability measurements (5000 cyclic voltammetric sweeps), as confirmed by Raman (Figure S17) and HRTEM (Figure S18) analysis. The high activity and durability of FeNi@NC demonstrate its great potential as a non-precious metal catalyst for OER.

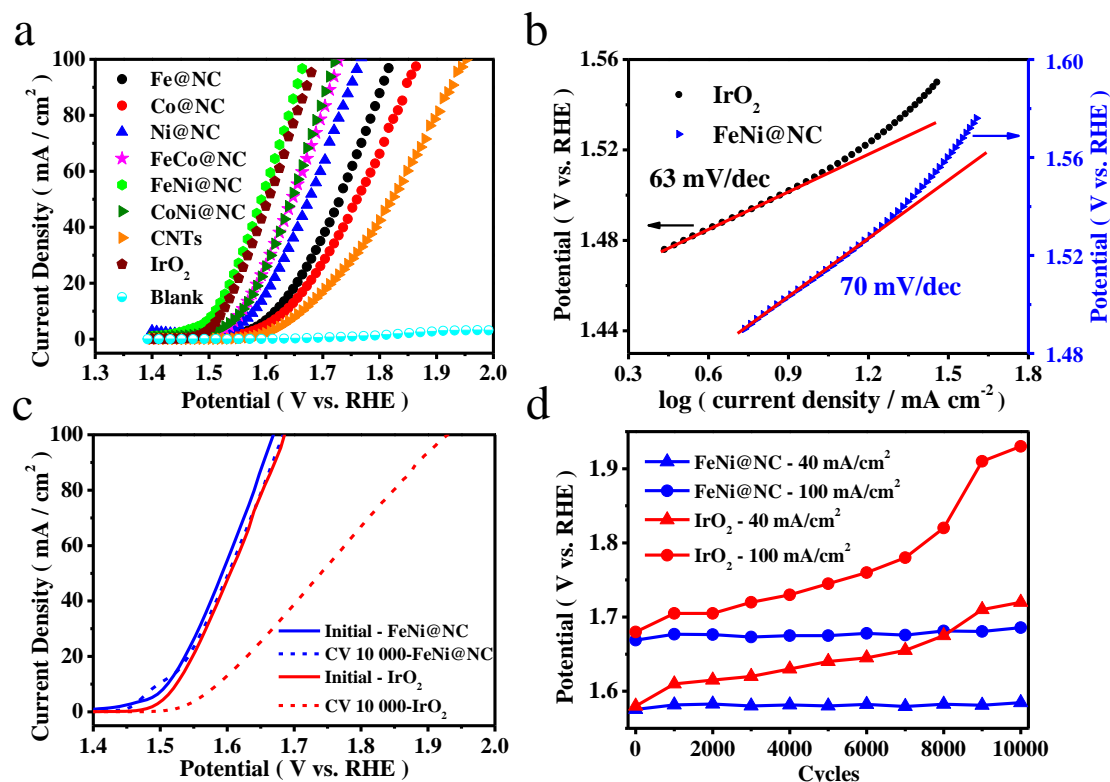
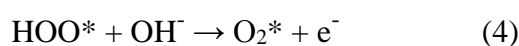
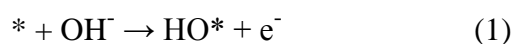


Figure 3. Electrocatalytic OER performance test of M@NCs in O₂-saturated 1 M NaOH solution at 25 °C. **(a)** OER polarization curves for M@NCs in comparison with CNTs and IrO₂ with same mass loading. **(b)** Tafel plots for FeNi@NC and IrO₂. **(c)** Durability test of FeNi@NC in alkaline electrolyte in contrast to IrO₂. **(d)** The potential changes of current densities at 40 mA cm⁻² and 100 mA cm⁻² for FeNi@NC and IrO₂ during the durability test.

In order to gain further insights into the nature of the M@NCs towards OER, density functional theory (DFT) calculations were employed. A graphitic carbon cage with 240 atoms encapsulating 55 metal atoms was used as the model of M@C. As shown in Fig 4a, it is generally agreed that OER involves the following steps³⁷, where the symbols “*” represent the active site.



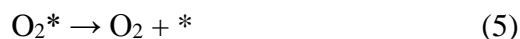


Fig 4b plot is the free energies of various intermediates for the OER catalyzed by FeNi@C at different constant potentials. It is shown that all reaction steps are endothermic at zero potential and the first three reaction steps are also endothermic at the equilibrium potential of 1.23 V, and until the potential increasing to 1.72 V, the free energies are downhill for all steps. This means that about 0.49 V overpotential compared with the equilibrium potential is needed for the OER process on FeNi@C. The analysis indicates that the calculated overpotential is determined by the free energies of the reaction intermediates HO*, O* and HOO*. Building the relation between free energies of intermediates and the overpotentials for various catalysts is vital to the rational design of catalysts^{38, 39}. Interestingly, as shown in Figure 4c, there is a good scaling relationship between the free energies of HO* and HOO* with a constant slope and intercept of 3.2 eV. The slope is equal to one, which implies that HO* and HOO* normally prefer the same bond type to the graphene surface, which is coincident with a wide range of oxides including rutile, perovskite, spinel, rocksalt and bixbyite and considered as a universal scaling relation³⁷. According to the scaling relation, the overpotential can only be determined by the free energy of O* relative to HO*, which is denoted as $\Delta G(\text{O}^*) - \Delta G(\text{HO}^*)$. With this established activity descriptor, the calculated overpotential exhibits a volcano shape, as shown in Fig 4d. The $\Delta G(\text{O}^*) - \Delta G(\text{HO}^*)$ of FeNi@C is 1.48 eV, which is closest to volcano peak among all the catalysts studied. Furthermore, Fig 4e plot is the comparison of calculated overpotential with experimental results, which agrees quite well in trend, indicating that our theoretical model is able to predict the efficiency of M@C in OER. The Bader charge analysis³⁸ in Table S5 indicated that the electronic properties of graphene shell can be significantly altered by electrons transferring from metal NPs, which further tune the binding energies of reaction intermediates on graphene surface. As a result, the OER descriptor $\Delta G(\text{O}^*) - \Delta G(\text{HO}^*)$ can be adjusted to the optimal value by changing the type of metal, such as Fe, Co, Ni and their alloys as shown in our experiments. Furthermore, introducing nitrogen into graphene layer can also tune the adsorption of reaction

intermediates and the corresponding reaction activity, as Noto et al. reported⁴⁰⁻⁴⁴. N-doping and enclosed metal cluster will synergistically enhance the adsorption of the intermediates as shown in Table S6. The increase of OER activity for the M@C samples in experiment (Figure S15) should be a compromise of the contribution of N-doped carbon and N-doped graphene encapsulating metal NPs, which are further discussed in supporting information (Fig S15 and Table S6) for simplicity.

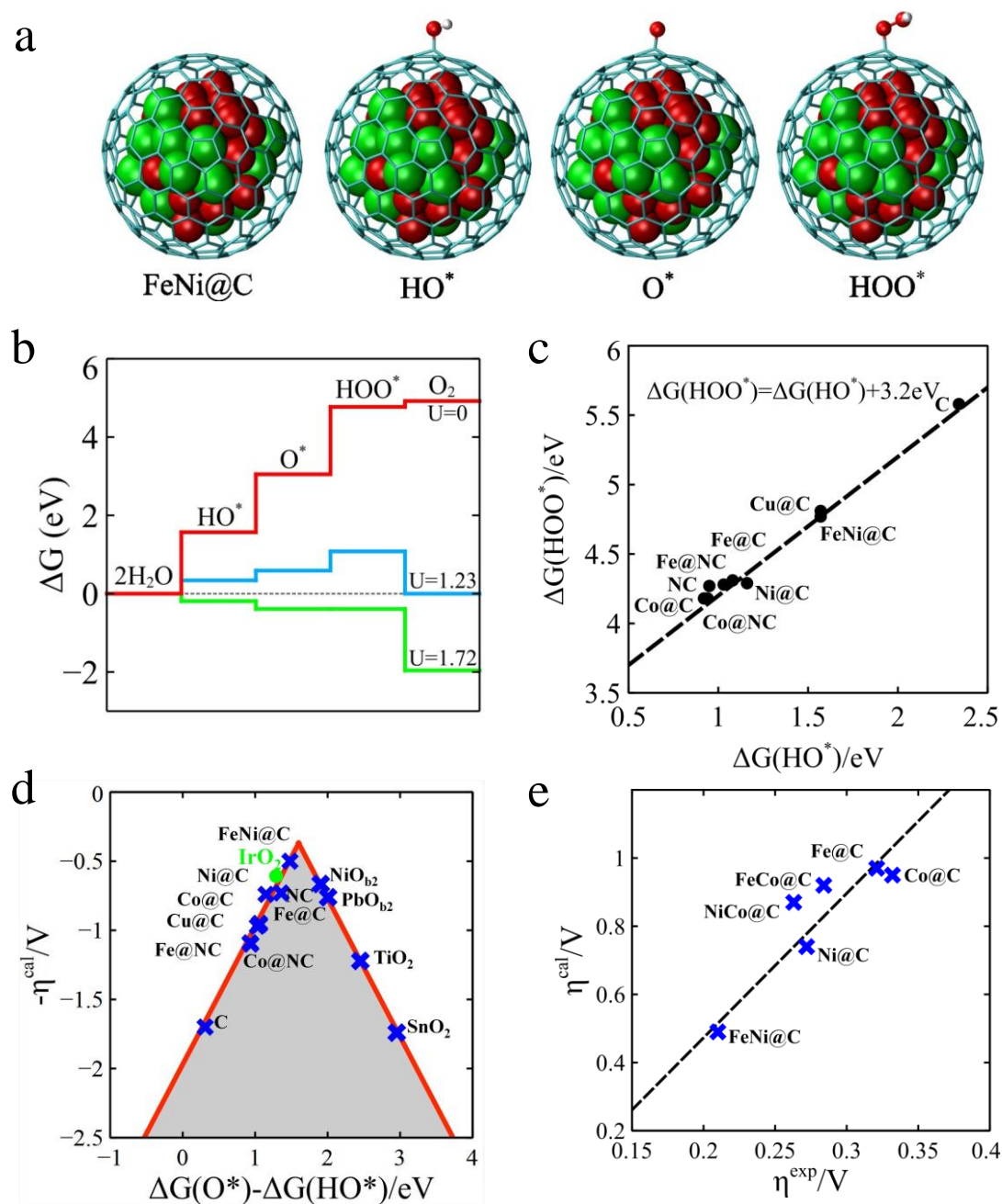


Figure 4. Theoretical interpretation of OER over M@Cs. (a) The OER steps on the

M@Cs models, where a graphitic carbon cage encapsulating 55 metal atoms. The grey cage, red and green balls represent C, Fe and Ni atoms, respectively. (b) Free energy profiles for the OER over FeNi@C at zero potential ($U = 0$), equilibrium potential for oxygen evolution ($U = 1.23$ V), and minimum potential ($U = 1.72$ V) where all steps become downhill. (c) Linear relation between the free energy of HO* ($\Delta G(\text{HO}^*)$) and HOO* species ($\Delta G(\text{HOO}^*)$) on different catalysts. (d) The calculated negative overpotential (η^{cal}) against the universal descriptor $\Delta G(\text{O}^*) - \Delta G(\text{HO}^*)$ on different catalysts. The data of oxides was cited from the literature by Man et al³⁷. (e) Calculated overpotential (η^{cal}) vs. the experimental overpotential (η^{exp}) over M@C catalysts. All experimental overpotential (η^{exp}) values were recorded at 2 mA cm^{-2} (Table S7).

In summary, we developed a facile and universal strategy to synthesize single layer graphene encapsulating 3d TMs, such as Fe, Co, Ni and their alloys through a CVD process in the channel of SBA-15. Electrochemical measurements indicated that different encapsulated metals have a different effect on the OER activity, and the optimized FeNi@NC catalyst showed the best activity with a high durability, both of which are superior to those of commercial IrO_2 . DFT calculations indicated that the high OER performance originates from the single layer graphene immensely promoting the electron transfer from the encapsulated metals to the graphene surface, which optimizes the electronic structure of the graphene surface and thereby triggers the OER activity on the inert graphene surface. These findings provide an efficient way towards the rational design of high-performance and low-cost OER electrocatalysts, as well as other energy-related catalysts.

References

1. Y. Jiao, Y. Zheng, M. Jaroniec and S. Z. Qiao, *Chem. Soc. Rev.*, 2015, **44**, 2060-2086.
2. A. Grimaud, K. J. May, C. E. Carlton, Y. L. Lee, M. Risch, W. T. Hong, J. Zhou and Y. Shao-Horn, *Nat. Commun.*, 2013, **4**, 2439.
3. R. Bashyam and P. Zelenay, *Nature*, 2006, **443**, 63-66.
4. C. Liu, F. Li, L. P. Ma and H. M. Cheng, *Adv. Mater.*, 2010, **22**, E28-62.
5. S. Mao, Z. Wen, T. Huang, Y. Hou and J. Chen, *Energy Environ. Sci.*, 2014, **7**, 609-616.
6. S. Chen, J. J. Duan, M. Jaroniec and S. Z. Qiao, *Angew. Chem. Int. Ed.*, 2013, **52**, 13567-13570.
7. X. Long, J. K. Li, S. Xiao, K. Y. Yan, Z. L. Wang, H. N. Chen and S. H. Yang, *Angew. Chem. Int. Ed.*, 2014, **53**, 7584-7588.
8. M. W. Louie and A. T. Bell, *J. Am. Chem. Soc.*, 2013, **135**, 12329-12337.
9. J. Wang, H. X. Zhong, Y. L. Qin and X. B. Zhang, *Angew. Chem. Int. Ed.*, 2013, **52**, 5248-5253.
10. S. M. Barnett, K. I. Goldberg and J. M. Mayer, *Nat. Chem.*, 2012, **4**, 498-502.
11. X. Lu and C. Zhao, *Nat. Commun.*, 2015, **6**, 6616.
12. F. Song and X. Hu, *Nat. Commun.*, 2014, **5**, 4477.
13. W. Zhou, X.-J. Wu, X. Cao, X. Huang, C. Tan, J. Tian, H. Liu, J. Wang and H. Zhang, *Energy Environ. Sci.*, 2013, **6**, 2921.
14. N. D. M. W. Chadwick Ellis, Stefan Bernhard, Terrence J. Collins, *J. Am. Chem. Soc.*, 2010, **132**, 10990-10991.
15. Q. S. Yin, J. M. Tan, C. Besson, Y. V. Geletii, D. G. Musaev, A. E. Kuznetsov, Z. Luo, K. I. Hardcastle and C. L. Hill, *Science*, 2010, **328**, 342-345.
16. Y. Y. Liang, Y. G. Li, H. L. Wang, J. G. Zhou, J. Wang, T. Regier and H. J. Dai, *Nat. Mater.*, 2011, **10**, 780-786.
17. S. Jin, J. M. Kevin, A. G. Hubert, B. G. John and S. H. Yang, *Science*, 2011, **334**, 1383-1385.
18. Z. Lu, H. Wang, D. Kong, K. Yan, P. C. Hsu, G. Zheng, H. Yao, Z. Liang, X. Sun and Y. Cui, *Nat. Commun.*, 2014, **5**, 4345.
19. T. Maiyalagan, K. A. Jarvis, S. Therese, P. J. Ferreira and A. Manthiram, *Nat. Commun.*, 2014, **5**, 3949.
20. D. H. Deng, L. Yu, X. Q. Chen, G. X. Wang, L. Jin, X. L. Pan, J. Deng, G. Q. Sun and X. H. Bao, *Angew. Chem. Int. Ed.*, 2013, **52**, 371-375.
21. J. Deng, P. J. Ren, D. H. Deng, L. Yu, F. Yang and X. H. Bao, *Energy Environ. Sci.*, 2014, **7**, 1919-1923.
22. J. Deng, P. J. Ren, D. H. Deng and X. H. Bao, *Angew. Chem. Int. Ed.*, 2015, **54**, 2100-2104.
23. X. Q. Chen, J. P. Xiao, J. Wang, D. H. Deng, Y. F. Hu, J. G. Zhou, L. Yu, T. Heine, X. L. Pan and X. H. Bao, *Chem. Sci.*, 2015, **6**, 3262-3267.
24. J. Deng, L. Yu, D. H. Deng, X. Chen, F. Yang and X. Bao, *J. Mater. Chem. A*, 2013, **1**, 14868-14873.
25. Y. Hu, J. O. Jensen, W. Zhang, L. N. Cleemann, W. Xing, N. J. Bjerrum and Q. Li, *Angew. Chem. Int. Ed.*, 2014, **53**, 3675-3679.
26. H. T. Chung, J. H. Won and P. Zelenay, *Nat. Commun.*, 2013, **4**, 1922-1926.
27. X. X. Zou, X. X. Huang, A. Goswami, R. Silva, B. R. Sathe, E. Mikmekova and T. Asefa, *Angew. Chem. Int. Ed.*, 2014, **53**, 4372-4376.
28. M. Tavakkoli, T. Kallio, O. Reynaud, A. G. Nasibulin, C. Johans, J. Sainio, H. Jiang, E. I. Kauppinen and K. Laasonen, *Angew. Chem. Int. Ed.*, 2015, **54**, 4535-4538.

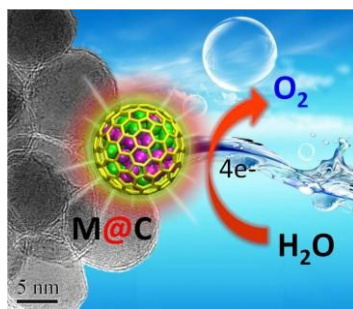
29. X. J. Zheng, J. Deng, N. Wang, D. H. Deng, W. H. Zhang, X. H. Bao and C. Li, *Angew. Chem. Int. Ed.*, 2014, **53**, 7143-7147.
30. T. Fu, M. Wang, W. M. Cai, Y. M. Cui, F. Gao, L. M. Peng, W. Chen and W. P. Ding, *ACS Catal.*, 2014, **4**, 2536-2543.
31. C. Wang, P. Zhai, Z. C. Zhang, Y. Zhou, J. Ju, Z. J. Shi, D. Ma, R. P. S. Han and F. Q. Huang, *Part. Part. Syst. Charact.*, 2015, **32**, 29-34.
32. B. Wang, M. Caffio, C. Bromley, H. Fr üchtl and R. Schaub, *Acs Nano*, 2010, **4**, 5773-5782.
33. F. Guinea, *Phys. Rev. B*, 2007, **75**, 235433.
34. P. A. Khomyakov, G. Giovannetti, P. C. Rusu, G. Brocks, J. van den Brink and P. J. Kelly, *Phys. Rev. B*, 2009, **79**, 195425.
35. G. Giovannetti, P. A. Khomyakov, G. Brocks, V. M. Karpan, J. van den Brink and P. J. Kelly, *Phys. Rev. Lett.*, 2008, **101**, 026803.
36. T. Olsen, J. Yan, J. J. Mortensen and K. S. Thygesen, *Phys. Rev. Lett.*, 2011, **107**, 156401.
37. I. C. Man, H. Y. Su, C. V. Federico, H. A. Hansen, J. I. Martínez, N. G. Inoglu, K. John, T. F. Jaramillo, J. K. Nørskov and R. Jan, *Chem. Cat. Chem.*, 2011, **3**, 1159-1165.
38. F. W. B. Richard, T. C. Marshall, J. R. Cheeseman and C. Cheng, *J. Am. Chem. Soc.*, 1987, **109**, 7968-7979
39. C. V. Federico, L. David, T. M. K. Marc and S. Philippe, *Nat. Chem.*, 2015, **7**, 403-410.
40. E. Negro, S. Polizzi, K. Vezzu, L. Toniolo, G. Cavinato and V. Di Noto, *Int. J. Hydrogen Energy*, 2014, **39**, 2828-2841.
41. V. Di Noto, E. Negro, S. Polizzi, F. Agresti and G. A. Giffin, *Chemsuschem*, 2012, **5**, 2451-2459.
42. E. Negro, K. Vezzu, F. Bertasi, P. Schiavuta, L. Toniolo, S. Polizzi and V. Di Noto, *Chemelectrochem*, 2014, **1**, 1359-1369.
43. V. Di Noto, E. Negro, S. Polizzi, K. Vezzu, L. Toniolo and G. Cavinato, *Int. J. Hydrogen Energy*, 2014, **39**, 2812-2827.
44. V. Di Noto, E. Negro, K. Vezzu, F. Bertasi and G. Nawn, *The Electrochemical Society Interface*, Summer 2015, **24**, 63-68.

Acknowledgements

We gratefully acknowledge the financial support from the National Natural Science Foundation of China (No. 21321002, 21573220 and 21303191) and the strategic Priority Research Program of the Chinese Academy of Sciences (No. XDA09030100). We thank Dr. Jianping Xiao for fruitful discussion.

Supporting information for this article is available on the WWW under <http://pubs.rsc.org/en/journals/journalissues/ee/> or from the author.

Entry for the Table of Contents



Single layer graphene encapsulating earth-abundant 3d transition metal nanoparticles shows excellent activity and durability for water oxidation, even exceeding IrO_2 .